Published in final edited form as:
Neuron. 2010 July 29; 67(2): 224–238. doi:10.1016/j.neuron.2010.07.001.

Modulation of High-Voltage Activated Ca^{2+} Channels by Membrane Phosphatidylinositol 4,5-Bisphosphate

Byung-Chang Suh[1,*], **Karina Leal**[2], and **Bertil Hille**[1]

[1]Department of Physiology and Biophysics, The University of Washington School of Medicine, Seattle, Washington 98195-7290, USA

[2]Department of Pharmacology and Program in Neurobiology and Behavior, The University of Washington School of Medicine, Seattle, Washington 98195-7290, USA

SUMMARY

Modulation of voltage-gated Ca^{2+} channels controls activities of excitable cells. We show that high-voltage activated Ca^{2+} channels are regulated by membrane phosphatidylinositol 4,5-bisphosphate (PIP_2) with different sensitivities. Plasma membrane PIP_2 depletion by rapamycin-induced translocation of an inositol lipid 5-phosphatase or by a voltage-sensitive 5-phosphatase (VSP) suppresses $Ca_V1.2$ and $Ca_V1.3$ channel currents by ~35%, and $Ca_V2.1$ and $Ca_V2.2$ currents by 29 and 55%, respectively. Other Ca_V channels are less sensitive. Inhibition is not relieved by strong depolarizing prepulses. It changes the voltage dependence of channel gating little. Recovery of currents from inhibition needs intracellular hydrolysable ATP, presumably for PIP_2 resynthesis. When PIP_2 is increased by overexpressing PIP 5-kinase, activation and inactivation of $Ca_V2.2$ current slow and voltage-dependent gating shifts to slightly higher voltages. Thus, endogenous membrane PIP_2 supports high-voltage activated L-, N-, and P/Q- type Ca^{2+} channels, and stimuli that activate phospholipase C deplete PIP_2 and reduce those Ca^{2+} channel currents.

Keywords

voltage-gated Ca^{2+} (Ca_V) channel; phosphatidylinositol 4,5-bisphosphate (PIP_2); voltage-sensitive phosphatase; rapamycin; muscarinic receptors

INTRODUCTION

Voltage-gated Ca^{2+} (Ca_V) channels mediate Ca^{2+} influx in response to membrane depolarization and regulate many physiological phenomena including neurotransmission, secretion, muscle contraction, and gene expression (Catterall et al., 2005). The activity of Ca_V channels is dynamically regulated by receptor-dependent signals, such as G proteins, protein kinases, calmodulin, soluble *N*-ethylmaleimide-sensitive fusion attachment receptor (SNARE) proteins, and the second messengers Ca^{2+} and arachidonic acid (Catterall, 2000; Dolphin, 2003; Roberts-Crowley et al., 2009). Here we analyze in detail the regulation of

Correspondence to: Byung-Chang Suh, Department of Physiology and Biophysics, University of Washington School of Medicine, Box 357290, Seattle, Washington 98195-7290, Tel.: 206-543-6661, FAX: 206-685-0619. *Correspondence: bcs@uw.edu.

SUPPLEMENTAL DATA

The Supplemental Data include 5 figures and the Supplementary Experimental Procedures listing the clones used.

three high-voltage activated (HVA) Ca^{2+} channels ($Ca_V1.2$, $Ca_V1.3$, and $Ca_V2.2$) by the plasma membrane phospholipid phosphatidylinositol 4,5-bisphosphate (PIP_2).

Signals from G-protein-coupled receptors (GPCRs) suppress N-type $Ca_V2.2$ channels through two pathways in sympathetic neurons (Hille, 1994). The “fast” pathway is voltage dependent, membrane delimited, and insensitive to the intracellular Ca^{2+} chelator BAPTA. The fast suppression is induced by activating receptors coupled to the pertussis toxin (PTX)-sensitive G proteins G_o and G_i. It can be relieved by applying large positive pulses (Bean, 1989; Lipscombe et al., 1989; Zamponi and Snutch, 1998), and is understood as direct voltage-dependent binding of G-protein βγ subunits to N-type ($Ca_V2.2$) and P/Q-type ($Ca_V2.1$) Ca^{2+} channels (Herlitze et al., 1996; Ikeda, 1996; Dolphin, 2003). By contrast, the “slow” pathway is voltage independent, insensitive to PTX, and sensitive to BAPTA. Activation of G_q-coupled receptors initiates the slow pathway (Bernheim et al., 1991; Delmas et al., 2005; Michailidis et al., 2007; Roberts-Crowley et al., 2009). While the fast and slow pathways both reduce the current appreciably, neither fully eliminates it. A phenomenologically similar slow pathway also produces inhibitory modulation of L-type Ca^{2+} channels and M-type (KCNQ) K^+ channels by G_q-coupled receptors in sympathetic neurons (Mathie et al., 1992) and in reconstituted systems (Shapiro et al., 2000; Bannister et al., 2002). We have speculated that the underlying signaling for slow suppression of these Ca^{2+} and K^+ channels might be the same (Bernheim et al., 1991; Mathie et al., 1992; Hille, 1994). Here we ask if some or all of the slow suppression of Ca^{2+} currents is due to receptor-mediated depletion of PIP_2 as is true for slow suppression of KCNQ K^+ current (Suh and Hille, 2002; Zhang et al., 2003; Brown et al., 2007).

Currents in the Ca_V2 channel family can be modulated by exogenous manipulation of membrane phosphoinositides (see reviews Delmas et al., 2005; Michailidis et al., 2007). Wu et al. (2002) concluded that depletion of membrane PIP_2 underlies a significant rundown of $Ca_V2.1$ (P/Q-type) currents seen in inside-out excised patch experiments. They showed that application of PIP_2 antibody to the intracellular side of giant membrane patches accelerates the $Ca_V2.1$ current rundown, whereas a brief application of PIP_2 or Mg-ATP retards the rundown. However, unexpectedly, they also reported that applied PIP_2 *reduced* the currents. The “inhibitory” effect of PIP_2 was actually a strong positive shift of channel voltage dependence (by ~40 mV). It was antagonized by conditions that activated cyclic AMP-dependent protein kinase. In subsequent studies, Gamper et al. (2004) reported that $Ca_V2.2$ N-type channels are also regulated by PIP_2. Macroscopic current rundown was significantly slowed by the application of PIP_2 to the intracellular side of excised membrane patches from *Xenopus* oocytes. In sympathetic neurons, the current suppression during muscarinic receptor activation was attenuated and slowed by intracellular perfusion of short-chain DiC_8-PIP_2. When the N-type Ca^{2+} currents were inhibited by G_q-coupled receptor activation, current recovery was blocked by 50 μM wortmannin, to inhibit PI 4-kinase. Thus, they proposed that depletion of PIP_2 on the plasma membrane is the cause of the G_q receptor-mediated slow inhibition of N-type Ca^{2+} currents in sympathetic neurons. The PIP_2 hypothesis has never been tested for L-, R-, or T- type channels in any system. In contrast, others have attributed the slow receptor-mediated inhibition of both N-type and L-type Ca^{2+} channels to production of arachidonic acid (Liu and Rittenhouse, 2003; Liu et al, 2006; Roberts-Crowley et al., 2009). Thus whether PIP_2 depletion is a major physiological signal for slow receptor-mediated suppression of N- and L-type Ca^{2+} channels remains controversial (Michailidis et al., 2007).

G_q-coupled receptor signals are notoriously difficult to dissect because they produce so many downstream second messengers. For example, in studies of G_q modulation of Ca^{2+} channels, PIP_2 depletion occurs simultaneously with the downstream production of arachidonic acid, activation of protein kinase C, and elevation of cytoplasmic free Ca^{2+},

which are all believed to have significant effects on the channels. In order to test the PIP_2 hypothesis unambiguously, we here use two strategies to deplete PIP_2 enzymatically and rapidly without producing the downstream products of PLC. We take advantage of two exogenous polyphosphoinositide 5-phosphatase systems that can convert $PI(4,5)P_2$ directly to PI(4)P in the plasma membrane in living cell systems without activation of receptors. One system uses "chemical dimerization," and the other uses membrane depolarization to activate transfected 5-phosphatase enzymes that convert PIP_2 to PIP. In chemical dimerization, addition of rapamycin or its analogue iRap to the extracellular medium induces irreversible translocation of a transfected yeast INP54p 5-phosphatase from cytosol to membrane, initiating PIP_2 dephosphorylation (Suh et al., 2006; Varnai et al., 2006). The translocation and dephosphorylation take 10 - 20 s. The other system uses a transfected voltage-sensitive phosphatase (VSP), an integral plasma membrane protein that becomes active when its N-terminal voltage-sensor domain detects large membrane depolarization (Murata et al., 2005; Halaszovich et al., 2008; Okamura et al., 2009). We find that the VSP system is faster, depleting plasma membrane PIP_2 within a second of activation, and the enzyme turns off quickly when the membrane is repolarized.

Here, we focus on the PIP_2 hypothesis and reserve examination of other messengers for later work. We consider N-type Ca^{2+} channels, which together with P/Q-type channels were the subject of the previous studies (Wu et al. 2002; Gamper et al. 2004; Lechner et al., 2005), and we consider two L-type channels whose PIP_2 dependence has not been studied before. In addition we screen the other subtypes of Ca_V channels. We find that PIP_2 depletion attenuates both L- and N-type Ca^{2+} channel activity through voltage-independent pathways, and increases the susceptibility of the channels to voltage-dependent inactivation (VDI). We also find that resynthesis of PIP_2 from PIP is needed for Ca_V channel recovery. Our experiments show that by itself PIP_2 depletion does depress HVA Ca^{2+} channel activity in living cells.

RESULTS

Our goal was to test the hypothesis that Ca^{2+} channels respond to depletion and resynthesis of PIP_2 in living cells. To establish conditions for recording Ca^{2+} channel currents, we expressed $Ca_V1.3$ (α1D) or $Ca_V2.2$ (α1B) channel subunits together with β3 and α2δ1 accessory subunits in tsA cells and recorded the whole-cell currents with Ba^{2+} as the charge carrier. Depolarizing voltage steps from a holding potential of −70 mV evoked inward currents carried by Ba^{2+} (Figure 1A). Barium was used to minimize Ca^{2+}-dependent inactivation of the current so that any current decay observed during the test pulses would be due primarily to voltage-dependent inactivation (VDI). As expected, the $Ca_V1.3$ currents inactivated little during the 40-ms test pulses, whereas the $Ca_V2.2$ currents inactivated more. Peak current-voltage (I-V) relations showed that $Ca_V1.3$ currents peaked near −10 mV (n = 6), whereas $Ca_V2.2$ currents peaked near +10 mV (n = 8) (Figure 1B). These respective peak voltages were used for all test pulses in subsequent experiments to assay the function of these channels, except where indicated.

Chemical Translocation of a PIP_2 5-phosphatase to the Plasma Membrane Attenuates Ca_V Currents

We begin with the chemical dimerization system and iRap to deplete membrane PIP_2. In addition to the channel subunits and the M_1 muscarinic receptor, two additional components needed to be co-transfected: the membrane-localized iRap-binding protein Lyn_{11}-FRB (LDR) and the fluorescent cytoplasmic enzyme construct CFP-FKBP-INP54p (CF-Inp). The CF-Inp has PIP_2 5-phosphatase activity that converts PIP_2 to PI(4)P. We showed previously that when LDR and CF-Inp are brought together at the membrane by application of iRap, PIP_2 is irreversibly depleted and PIP_2-dependent KCNQ K^+ channels turn off (Suh et al.,

2006). This system is suitable for experimental designs that benefit from the irreversible PIP_2 depletion that follows chemical dimerization.

As an initial control, when CF-Inp is expressed but the membrane anchor LDR is omitted (−LDR), iRap had little direct effect on the currents (top panels in Figures 1C and 1D), although both channels were readily inhibited by M_1 receptor activation with the muscarinic agonist Oxo-M. When LDR was included (+LDR) there were two changes. First, currents in Ca^{2+} channels were decreased irreversibly by iRap (bottom panels in Figures 1C and 1D), a decrease that was less than had been seen with muscarinic receptor activation. The second effect was alteration of the subsequent response to muscarinic receptor activation. Prior PIP_2 depletion by activated INP54p 5-phosphatase eliminated further inhibition of $Ca_V1.3$ current by muscarinic receptors (Figure 1C), quite possibly because the irreversible depletion of PIP_2 abrogates muscarinic generation of all PIP_2 cleavage products, including inositol trisphosphate and calcium signaling (Suh et al., 2006). On the other hand, further muscarinic modulation of $Ca_V2.2$ current remained intact and reached full amplitude (Figure 1D). Quite possibly that pathway does not require PIP_2. It might involve G protein βγ subunits or other products of phospholipases including PLA_2 (Melliti et al., 2001; Roberts-Crowley et al., 2009). As a preliminary conclusion, muscarinic inhibition of both channels probably occurs via more than one pathway, and any PIP_2 depletion component accounts for only part of the total effect.

It is well known that inhibition of $Ca_V2.2$ current by M_2 muscarinic receptor-mediated signaling (the fast Gβγ pathway) is strongly relieved by large positive prepulses (Elmslie, et al., 1990). We readily verified this effect in cells transfected with M_2 (G_i-coupled) rather than M_1 (G_q-coupled) receptors (data not shown). Can the iRap-induced inhibition of $Ca_V1.3$ and $Ca_V2.2$ channels also be relieved by strong depolarizing prepulses? The cells were given a +130-mV/20-ms prepulse followed 5 ms later by a 10-ms test pulse to measure channel function. Figure S1 shows that inhibition was unchanged by the prepulses for $Ca_V1.3$ channels (Figure S1A) and for $Ca_V2.2$ channels (Figure S1B). Hence, unlike inhibition of $Ca_V2.2$ channels via Gβγ, positive prepulses do not relieve the suppression that follows iRap-induced PIP_2 depletion.

Depletion of Membrane PIP_2 by Activation of Dr-VSP Attenuates Ca_V Currents

We turn now to depleting PIP_2 with the voltage-sensitive phosphatase from zebra fish (Dr-VSP; Okamura et al., 2009). This tool is suitable for experimental designs that benefit from reversible PIP_2 depletion following an activating depolarization. First we characterized the ability of Dr-VSP to deplete membrane PIP_2 by using two fluorescent PIP_2 indicators and measuring fluorescence resonance energy transfer (FRET) between them (van der Wal, 2001; Jensen et al. 2009). In resting cells, the PIP_2-binding fluoroprobes CFP-tagged PH(PLCδ1) and YFP-tagged PH(PLCδ1) bind to the PIP_2 at the plasma membrane in high enough surface density to generate FRET between them (Figure S2A). If PIP_2 is depleted, the probes dissociate from the membrane and move to the cytosol, losing their FRET interaction (van der Wal et al., 2001). In cells cotransfected with Dr-VSP, application of depolarizing pulses to +120 mV activated the phosphatase activity. Using 440-nm light to excite CFP, the fluorescence of CFP (CFP_C) increased and that of YFP (YFP_C) decreased each time the depolarization was applied (Figure S2B, top), and PIP_2 depletion was signaled as the corresponding decrease in the FRET ratio (FRET ratio = YFP_C/CFP_C) (Figure S2B, bottom). During the large depolarization, the PIP_2 depletion developed rapidly (exponential time constant $\tau = 105 \pm 18$ ms, n = 9) (Figure S2C) and in a voltage dependent manner ($V_{1/2} = 61 \pm 5$ mV, n = 5) (Figure S2D). According to the FRET assay, the depletion with Dr-VSP is comparable to that seen with M_1 muscarinic receptor activation (Figure S2E). However, it is much faster and results in quite different cleavage products.

As was anticipated from the PIP_2 depletion, activation of Dr-VSP decreased current in HVA Ca^{2+} channels. Our protocol was to apply a standard test pulse (pulse a) to record baseline channel current, then a large depolarizing pulse for various times to activate Dr-VSP, followed by a second test pulse (pulse b) (Figure 2A). In control cells not expressing Dr-VSP, $Ca_V1.3$ current amplitudes a and b were almost the same without (0 s) or with (0.5 s) a 0.5-s depolarization to +120 mV (Figure 2A, left). In contrast, in cells expressing Dr-VSP, the 0.5-s depolarizing pulse significantly attenuated the Ba^{2+} current in pulse b (Figure 2A, middle). Again, in the same cell there was no significant change in current b without the large pulse. To examine whether this Dr-VSP-induced inhibition of $Ca_V1.3$ current is caused by PIP_2 degradation, we tested the effect of Dr-VSP activation in cells transfected with the PIP 5-kinase type-1γ (PIPKIγ). This enzyme elevates PIP_2 concentration in the plasma membrane (Wenk et al., 2001) and thereby diminishes the ability of G_q-coupled receptors to suppress KCNQ K^+ currents (Suh and Hille, 2007). As shown in Figures 2A and 2C right, the inhibition of $Ca_V1.3$ and $Ca_V2.2$ channels by Dr-VSP was significantly attenuated by PIPKIγ expression. Figure 2B plots the time dependence of the b/a current ratio (top) and of the percent inhibition with and without Dr-VSP (bottom). The $Ca_V1.3$ channels were maximally inhibited by 33% with an onset time constant $\tau = 112 \pm 7$ ms (Figure 2B, bottom left). Further, PIPKIγ overexpression significantly attenuated the Dr-VSP-induced $Ca_V1.3$ inhibition (Figure 2B, top left).

We also performed Dr-VSP experiments with N-type $Ca_V2.2$ channels. The bottom line was similar: $Ca_V2.2$ channels were inhibited by Dr-VSP activation with a maximum inhibition of 56% and onset $\tau = 143 \pm 10$ ms (Figure 2D, bottom). However, in these experiments there was much more evidence of channel inactivation induced by the voltage protocols. Even in the absence of Dr-VSP, the $Ca_V2.2$ current in pulse b was reduced by as much as 31 ± 2% (n = 6) by the preceding 0.5-s depolarization to +120 mV (Figures 2C and D). Moreover, N-current was even partially reduced without (0 s) the large depolarizing pulse. To compensate for such “control” inactivation, we calculated the percent inhibition due to Dr-VSP action by the formula $100\ \{1 - (b/a)_{VSP}/(b/a)_{Control}\}$ at each time point in this figure and in subsequent figures. This correction would apply accurately if the “inactivation” seen without Dr-VSP is unchanged by the action of Dr-VSP, an assumption that we revisit later. Hence, Dr-VSP, like the iRap-dimerizable INP54p system, depletes PIP_2 and leads to parallel depression of currents in three subtypes of Ca^{2+} channels. We did find that, for $Ca_V1.3$ and $Ca_V2.2$ channels, the mean inhibition by Dr-VSP was ~35% larger than that with the iRap system. In summary, experiments with two lipid phosphatases are consistent with the hypothesis that PIP_2 regulates Ca_V channels.

Inhibition of Ca_V Channels by Dr-VSP Is Not Simple VDI

We have already said that much of the current inactivation developing during test pulses in the presence of barium is voltage-dependent, VDI. In Figure 3 we examined the role of VDI in our measurements and its possible dependence on PIP_2. We ask whether some parts of the inhibition by Dr-VSP are simply an enhancement of VDI by testing whether the inhibition can be removed by a large hyperpolarizing pulse. The 0.9-s hyperpolarizing voltage step to −150 mV ended 0.1 s before test pulse b (see pulse protocols in Figures 3A and 3C).

In control cells, $Ca_V1.3$ currents showed no or very minor VDI from the +120-mV/1-s depolarizing pulse, i.e., in control cells, currents a and b were very similar even without the hyperpolarization. With the −150-mV hyperpolarizing voltage step, the minor VDI was abolished (Figure 3A, top right). In cells expressing Dr-VSP, $Ca_V1.3$ current b was strongly reduced compared to a, without and with the hyperpolarizing step (Figures 3A, bottom, and 3B). Thus, $Ca_V1.3$ channels had little residual VDI from our pulse protocol, and the inhibitory effect of Dr-VSP activation was not relieved by hyperpolarizations. In control cells expressing $Ca_V2.2$ channels, there was some residual VDI after pulse a (Figure 3C, top

left). This made the pulse b currents ~30% smaller (Figures 3C and 3D). The reduction was totally relieved by the −150-mV/0.9-s hyperpolarization. Indeed, the current in pulse b became larger than that in pulse a as if the hyperpolarization was also relieving some resting inactivation that had reduced pulse a current (Figure 3C, top right). With Dr-VSP, the large depolarizing pulse strongly depressed current in pulse b as before. Again when compared to the control cells, the hyperpolarizing step did not relieve any of the effect of VSP (Figure 3D). $Ca_V2.2$ channels show prominent tail currents. Therefore, we also could test whether the tail currents were inhibited by Dr-VSP. Figures 3E and F show strong inhibition in Dr-VSP expressing cells. The inhibition of tail currents was similar to that of inward currents during test pulses. Thus for $Ca_V1.3$ and $Ca_V2.2$ channels, the depression of current due to Dr-VSP activation did not seem to be some kind of enhancement of VDI.

Subtype-Specificity of PIP_2 Modulation of Ca_V Channels

We screened for channel modulation by expressing different α_1 subunits with the same β3 and α2α1 channel subunits as before. Figure 4A shows that the $Ca_V1.2$ and $Ca_V2.1$ channel currents were also significantly inhibited by Dr-VSP activation although less than for $Ca_V2.2$ channels. Since the current-voltage relations for $Ca_V1.2$ and $Ca_V2.1$ peaked at +10 mV and 0 mV, respectively (Figure S3A), those voltages were used for the test pulses in these experiments. The $Ca_V1.2$ channels gave currents similar to those with $Ca_V1.3$ and showed almost the same inhibition by muscarinic activation (62 ± 8% for $Ca_V1.2$, n = 5; 59 ± 3% for $Ca_V1.3$, n = 6) (Figures 4B and 4C, bottom). Furthermore, the effects of Dr-VSP activation were very similar (Figure 4C, top). With $Ca_V1.2$ channels, the large depolarizing pulse produced a 35% inhibition of current developing with an onset time constant τ = 138 ± 18 ms (n = 6). $Ca_V2.1$ channels are inhibited by both Dr-VSP and M_1 receptor stimulation (Figure 4). However, the other subtypes of Ca_V channels, 1.4, 2.3, and all Ca_V3 (T-type), were insensitive to Dr-VSP activation (Figures 4C and S3B). Interestingly, the four PIP_2-depletion-sensitive channels were also strongly inhibited by M_1 receptor activation with Oxo-M, and the other channels were not significantly inhibited by Oxo-M. Indeed $Ca_V2.3$ R-type currents were strongly enhanced (Figure S3C).

PIP_2 Dependent Modulation of $Ca_V2.2$ Channels

PIP_2-dependence of Ca_V current modulation was investigated in more detail with $Ca_V2.2$ channels. When the cells overexpressed the PIP_2-binding peptide scavenger, PH domain of PLCδ1, the current density in the transfected cells was significantly decreased compared to control cells expressing only GFP or cells expressing PH domain of Akt protein which binds to $PI(3,4)P_2$ and PIP_3 in the plasma membrane (Figure 5A). Next we tested if PIP_2 elevation above its normal level attenuates the muscarinic suppression of the $Ca_V2.2$ channels. Overexpression of PIPKIγ significantly attenuated the M_1 muscarinic receptor-induced inhibition (Figure 5B) as well as the Dr-VSP-induced $Ca_V2.2$ inhibition (Figure 2C). The muscarinic inhibition without PIPKIγ was 72 ± 8% (n = 6), and with PIPKIγ it was reduced to 35 ± 7% (n = 6).

Finally, we tested if PIP_2 depletion could decrease the endogenous $Ca_V2.2$ N-type current of sympathetic superior cervical ganglion (SCG) neurons. Figure 5C shows the current-voltage relationship of N-type current in SCG neurons expressing Dr-VSP. The current peaked at ~10 mV. When the Dr-VSP was activated by +120 mV/1 s-depolarization, it inhibited the N-type current by 28% in SCG neurons (Figure 5D). Thus membrane PIP_2 is also important for Ca_V channel activity in differentiated neurons.

Recovery from Dr-VSP-Induced Inhibition Requires Intracellular ATP and PIP_2 Resynthesis

After the Dr-VSP-induced inhibition, current recovered in < 1 min. We tested the need for PIP_2 synthesis in channel recovery. Current was elicited with the voltage protocols shown in

Figures 6A and 6E. Cells were given a 10-ms test pulse to measure the initial current (I_0), then depolarized to +120 mV for 1 s to activate Dr-VSP. Finally, recovery from inhibition was measured by applying 10-ms test pulses with successively longer delay after VSP activation starting at 0.5 s as indicated above the traces. As before, in control cells expressing $Ca_V1.3$ channels, the current was only slightly inhibited by the large depolarizing pulse (Figure 6A, top). With Dr-VSP, the $Ca_V1.3$ current was reduced by the depolarization and recovered to the initial level with a recovery time constant τ of 5.9 s (Figures 6A, bottom, and 6B). In control cells expressing $Ca_V2.2$ current, the current was reduced by VDI and then recovered (Figure 6E, top). In cells with Dr-VSP, the current was strongly inhibited by the large depolarization and, after correcting for control VDI, recovered with a time constant τ of 16.1 s (Figures 6E, bottom, and 6F), slower than for $Ca_V1.3$ channels. The slower recovery of $Ca_V2.2$ compared to $Ca_V1.3$ did not seem to be due to some form of slowly recovering VDI, since it was not significantly relieved or speeded by a −150-mV hyperpolarizing step (Figure S4A).

We next tested the hypothesis that PIP_2 resynthesis is needed for Ca_V current recovery from the Dr-VSP-induced inhibition. First we speeded resynthesis. Coexpression of the 5-kinase PIPKIγ with$Ca_V1.3$ or $Ca_V2.2$ channels significantly decreased the current inhibition with the +120-mV/1-s pulse and speeded the current recovery (Figures 6B, 6C, 6F, and 6G). Next we slowed PIP_2 resynthesis. The synthesis of PIP_2 from PI(4)P requires intracellular ATP, so we slowed the kinase activity by dialyzing the nonhydrolyzable ATP analogue AMP-PCP into the cell. The inclusion of 3 mM AMP-PCP instead of ATP in the pipette solution did not significantly affect maximum channel inhibition, but strongly slowed the recovery of both $Ca_V1.3$ current (τ = 21 s) (Figure 6D) and $Ca_V2.2$ current (τ = 32 s) (Figure 6H) and diminished the maximum recovery (for traces, see Figure S4B). As expected, dialyzing with AMP-PCP also strongly slowed and depressed PIP_2 resynthesis as measured by FRET with PH-domain probes (Figure S4C). With ATP, the Dr-VSP-induced FRET ratio changes recovered almost completely (94 ± 3%) with a time constant τ of 6.4 ± 0.9 s (n = 11), whereas with 3 mM AMP-PCP the recovery after one large depolarizing pulse was smaller (only 58 ± 3%) and slower with a time constant τ = 32 ± 4 s (n = 5), and there was no recovery after a second depolarizing pulse as if the last remaining ATP had been exhausted (Figure S4D). Inclusion of another nonhydrolyzable ATP analogue AMP-PNP gave a similar retardation of the FRET recovery (data not shown). In summary, we find that channel recovery after PIP_2 depletion is faster when PIP_2 synthesis is speeded and slower and incomplete when PIP_2 synthesis is slowed, implying that PIP_2 resynthesis underlies Ca_V channel recovery from the VSP-mediated inhibition.

Simultaneous Measurements of Channel Modulation and PIP_2 Degradation in the Same Cells

A puzzling finding was that recovery of $Ca_V1.3$ channels (Figure 6) closely paralleled that of FRET ratio measured in separate experiments (Figure S2), whereas recovery of $Ca_V2.2$ channels was slower than that of FRET ratio. Could it be that because we studied one set of cells expressing PH domains and different sets of cells expressing the channels, the comparison was not valid? It seemed necessary to cotransfect PH domains and channels and to measure the current and FRET ratio simultaneously in the same cell.

The following experiments show in simultaneous recordings, that the close parallels between Dr-VSP effects on $Ca_V1.3$ currents and FRET ratio changes persist. Figure 7A measures the onset of the Dr-VSP effects with depolarizations of different duration (Δt). The duration dependence was indistinguishable (Figure 7A, bottom), and the ratio of the time constants for onset (τ current /τ FRET) was 1.02 ± 0.09 (n = 5). Figure 7C shows the dependence on the voltage of the pulse for VSP activation; the mid-point voltage was 58 mV for both responses. Similarly, the recovery time courses of current and FRET ratio after

termination of the depolarizing pulse were the same (time constant ratio 0.91 ± 0.09, n = 5; Figure 7D); when AMP-PCP replaced ATP in the pipette, the recoveries remained parallel although much slowed (Figure 7F). On the other hand, in similar simultaneous recording experiments with $Ca_V2.2$ channels, differences in time course persisted. The duration dependence for onset showed quicker loss of current than of FRET ratio (time constant ratio 0.65 ± 0.04, n = 4; Figure 7B) and the recovery after Dr-VSP showed slower recovery of current (time constant ratio 3.7 ± 0.7, n = 6; Figure 7E). These ratios ought to be interpreted cautiously since it was not possible to correct for confounding VDI in these experiments.

Modulation of $Ca_V2.2$ Currents by Dr-VSP is not Gβγ binding

$Ca_V2.2$ (N-type, α1B) channel currents can be suppressed by membrane Gβγ subunits in a voltage-dependent manner (Dolphin, 2003). Might the Dr-VSP-mediated channel modulation be due in part to enhanced binding of Gβγ subunits to $Ca_V2.2$ channels when membrane PIP_2 is depleted? As a test we took advantage of the Gβγ subunit-insensitive chimeric channel construct called α1C-1B (Agler et al., 2005). In this construct, the N-terminus of $Ca_V2.2$ (N-type, α1B subunit), which includes one of the Gβγ binding sites, is replaced by the N-terminus of $Ca_V1.2$ (L-type, α1C subunit) (Figure 8A). When expressed in tsA cells, these chimeric channels activated in the same voltage range as wild type $Ca_V2.2$ channels but could not be inhibited by stimulation of M_2 (G_i-coupled) muscarinic receptors (Figures 8B and 8C). The wild type $Ca_V2.2$ channels were readily inhibited (78 ± 5%, n = 5). In cells expressing the chimeric channels and Dr-VSP, a +120-mV/1-s depolarizing pulse strongly inhibited the current by 56% when corrected for VDI seen in control cells (Figures 8D and 8E). Following the inhibition, the chimeric channels recovered with a time constant τ of 15 s (Figure 8F), comparable to the wild type channels (Figure 6F). These experiments give no evidence for enhanced binding of Gβγ subunits to the channel when PIP_2 is depleted. They also show that replacing the N-terminus of the $Ca_V2.2$ with that of $Ca_V1.2$ subunits does not change PIP_2-mediated channel modulation.

Does PIP_2 Depletion Change Channel Gating Properties?

A preliminary examination revealed only modest effects on channel gating as plasma membrane PIP_2 was depleted or raised. Some speeding of the development of VDI by PIP_2 depletion is shown in Figure 9A, again using our a/b pulse protocols but with longer test pulses. In control cells without Dr-VSP, the +120-mV/1-s depolarizing pulse had no effect on the time constant of VDI development during the subsequent 500-ms test pulse (Figure 9A, top panels). For $Ca_V1.3$ channels, the time constant (τ) of inactivation was 200 ± 27 s (n = 5) vs. 193 ± 22 s (n = 5), in pulses a and b, respectively, and for $Ca_V2.2$ channels, τ values were 44 ± 1 s vs. 42 ± 1 s (n = 5). However, with Dr-VSP, the time constant of inactivation was shortened, especially for $Ca_V2.2$ channels (49 ± 4 s vs. 25 ± 2 s for currents a and b, n = 5, *P < 0.001) (Figure 9A, bottom right). We note that test-pulse depolarizations to +10 mV produced no change in PH-domain FRET signals and thus do not activate Dr-VSP (Figure S2D). For $Ca_V2.2$ channels, we also explored effects of an increase in membrane PIP_2 levels by over-expressing the enzyme PIPKIγ. With elevated PIP_2, the development of VDI was slowed by ~1.7-fold at +10 mV and slowed by ~2-fold at +30 mV compared to control (Figures 9B and 9C). The *activation* of $Ca_V2.2$ channels was also slowed with expression of PIPKIγ, delaying the time to peak current (Figures 9D, S5A and S5B). Finally, effects on the voltage dependence of activation were small. When PIP_2 was depleted by the combination of Dr-VSP and AMP-PCP, the voltage dependence of activation of $Ca_V1.3$ channels was not changed and that for $Ca_V2.2$ channels showed a statistically insignificant left shift (Figure S5C and S5D). On the other hand, when PIP_2 was augmented by PIPKIγ, the current-voltage relation for $Ca_V2.2$ channels was significantly right shifted by 5-7 mV (Figure 9E). None of these small gating changes is sufficient to account for the large depression of currents that

we have described following PIP_2 depletion. Rather it seems that with reduced PIP_2, fewer Ca_V channels are available to open.

DISCUSSION

Using direct enzymatic methods to modify PIP_2 levels quickly in living cells, we have developed compelling support for the hypothesis that the endogenous PIP_2 of a cell maintains a high activity of $Ca_V1.2$, $Ca_V1.3$, $Ca_V2.1$, and $Ca_V2.2$ channels and that physiological reductions of PIP_2 immediately decrease the channel activity: (1) Irreversible depletion of endogenous membrane PIP_2 using iRap-induced translocation of INP54p 5-phosphatase to the plasma membrane irreversibly decreased the whole-cell Ca_V currents. (2) Reversible depletion of membrane PIP_2 by the activation of Dr-VSP reversibly decreased Ca_V currents in less than 1 s, with little change in voltage-dependent channel gating. (3) Elevating levels of membrane PIP_2 by transfecting with PIP 5-kinase significantly blunted the channel inhibition by Dr-VSP and accelerated recovery from inhibition ~4-fold. (4) Attenuating the endogenous PIP 5-kinase activity using nonhydrolyzable ATP analogs had parallel inhibitory effects on measured PIP_2 resynthesis and on recovery of channels from inhibition. And (5) the Dr-VSP-mediated PIP_2 depletion and the channel inhibition, as well as subsequent PIP_2 resynthesis and channel recovery, developed with similar time courses in single cells. This correspondence was especially tight for $Ca_V1.3$ channels. The loss of $Ca_V1.3$ current tracks the loss of PIP_2 within milliseconds. Together these new observations show that the activities of several HVA Ca_V channels depend on endogenous membrane PIP_2 in intact cells. This is the first direct evidence that L-type channels participate in such regulation. As a caveat, we note that we are reporting tests with the β3 and α2δ1 accessory subunits and specific splice variants of the α1 subunits. Since several forms of channel modulation are known to be affected by the subtypes of each subunit, the quantitative conclusions here can be applied strictly only to the subunits we actually tested (e.g., Raingo et al., 2007).

Membrane PIP_2 is a Modulatory Cofactor for Ca_V Channel Activity

The central question that motivated our study is whether a downstream signal of PLCβ, PIP_2 depletion, is important for signaling to Ca_V channels. We have studied the most prominent Ca_V channel types of native rat SCG neurons α1B/β3/α2δ1 ($Ca_V2.2e[37b]$) and α1D/β3/α2δ1 ($Ca_V1.3e$) (Lin et al., 1996; Bell et al., 2004) in reconstituted systems. Our data show how membrane PIP_2 turnover modulates these HVA Ca_V channels in living cell membranes and reveal similarities and novel differences between various subtypes of Ca_V channels in the modulation by PIP_2. The activity of these channels is significantly decreased by conversion of PIP_2 to PIP and remains inhibited until the PIP_2 is resynthesized from PIP by endogenous PIP 5-kinases. Thus the anionic phosphoinositide PIP_2 is a cofactor required for full channel activity. Our data suggest that the channels must be in equilibrium with plasma membrane pools of PIP_2 on a time scale much shorter than the 100 ms that it takes for Dr-VSP to depress their currents. There must be a protein-lipid binding interaction of low affinity. The short time intervening between PIP_2 dephosphorylation and the channel response argues against indirect actions such as downregulation of channels by endocytosis. The magnitude of inhibition is greater via M_1 receptors than with exogenous 5-phosphatase-dependent PIP_2 depletion.

Our experiments with intact cells did not duplicate all the phenomena reported for excised patches with $Ca_V2.1$ and $Ca_V2.2$ channels (Wu et al., 2002; Gamper et al., 2004). In the excised patch experiments, tail currents ran down nearly 100% in 2 min, and almost all of the tail current could be restored by direct addition of PIP_2. Further, the addition of PIP_2 induced a rightward shift by ~40 mV in the voltage dependence of channel activation. Finally the rightward shift was blocked in conditions favoring phosphorylation by cAMP-

dependent protein kinase. In the intact-cell experiments of Gamper et al. (2004) and in our experiments, depletion of PIP_2 suppressed current only partially and any rightward shift with excess PIP_2 was <10 mV. Perhaps in whole-cell experiments, some channel phosphorylations are preserved, or possibly other cytoplasmic factors make the channels less drastically PIP_2 sensitive. Perhaps also continuing PIP_2 synthesis prevents full depletion of the PIP_2. Indeed, when we did experiments with non-hydrolyzable ATP analogues, the inhibition by VSP tended to be larger and cumulative.

Activating Dr-VSP removes the 5 phosphate from PIP_2 and produces a transient rise of membrane PI(4)P that then decays as it is converted back into PIP_2 (Halaszovich et al., 2009). Our finding that channel currents fall during the transient PIP_2 depletion means that PI(4)P is not as effective as PIP_2 in supporting channel activity. Since currents are inhibited by only 33-60% for the three channels studied, it is still possible that the elevated PI(4)P or other acidic phospholipids also support channel activity but significantly less well than resting levels of PIP_2. Direct experiments with other enzymes would be needed to test that hypothesis.

In our experiments, N-type channels were inhibited more than L-type channels by PIP_2 depletion, both by iRap-induced translocation and by Dr-VSP. Unexpectedly, the maximum inhibition by Dr-VSP was ~25-35% larger than the inhibition by iRap-induced phosphatase translocation. We suggest that the difference arises from a small basal PIP_2 5-phosphatase activity of the translocatable INP54p that partially depletes membrane PIP_2 already before rapamycin is added. According to our kinetic models (Suh et al, 2004), even a 1% resting activity at the membrane would lower the PIP_2 level by 20%, enough to reduce the channel currents partially. This would make the subsequent iRap-induced inhibition smaller. Thus, we estimate using the Dr-VSP results that about 55% of $Ca_V2.2$ and 35% of $Ca_V1.2$ and $Ca_V1.3$ current is lost when endogenous PIP_2 is depleted. By comparison, about 75% of $Ca_V2.2$ and 55-65% of $Ca_V1.2$ and $Ca_V1.3$ current is lost when M_1 muscarinic receptors are activated. We propose that a significant fraction but not the entire muscarinic inhibition is due to PIP_2 depletion. Previously, we and others showed that activation of M_1 or M_3 muscarinic receptors significantly depletes membrane PIP_2 (Willars et al., 1998; Horowitz et al., 2005; Winks et al. 2005; Jensen et al., 2009). The depletion is >>90% as assayed by translocation or loss of FRET from PH-domain probes and by direct biochemical methods. In this multiple-pathway theory of muscarinic inhibition, there would also be several components to the post-agonist recovery as each of the underlying messenger systems make its own recovery. Commonly discussed additional candidate messengers that do act on Ca_V1 or Ca_V2 family channels are divalent ions, Gβγ subunits, arachidonic acid, and protein kinase C (Delmas et al., 2005; Michailidis et al., 2007; Roberts-Crowley et al., 2009). The alternative hypothesis, which we regard as unlikely on kinetic grounds, is that stronger inhibition by PLC simply reflects an inability of our phosphatases tools to deplete PIP_2 as much as PLC does.

Mechanisms for the PIP_2 actions on Ca_V channels

What is PIP_2 loss doing to channels to decrease the net current they carry? We considered two possibilities with negative results. We considered whether PIP_2 loss makes channels more susceptible to modulation by Gβγ subunits. This possibility seems unlikely both because the PIP_2 effect was unchanged in mutant channels where the Gβγ binding site was crippled and because the inhibition by PIP_2 depletion was not relieved by large positive "facilitating" pulses the way Gβγ inhibition would be. We also considered whether PIP_2 loss enhances VDI enough to account for the suppression of Ca^{2+} currents. Although PIP_2 depletion did speed development of VDI, and PIP_2 augmentation slowed it, the component of inhibition due to PIP_2 depletion was not reversed by large hyperpolarizing conditioning pulses that were sufficient to remove normal VDI.

Our kinetic results with Dr-VSP suggest that $Ca_V1.3$ channel activity follows changes in the membrane PIP_2 level closely in a simple linear manner. They can be described by a model with low-affinity, rapid, first order, non-cooperative binding of PIP_2 to $Ca_V1.3$ channels, where each bound PIP_2 contributes a certain increment to the channel activity. Our data would be consistent with a model having only one facilitatory PIP_2 site on $Ca_V1.3$ channels, but there also could be several. The $Ca_V2.2$ channels behave differently. Their activity possibly falls faster than PIP_2 is depleted and certainly recovers much slower than PIP_2 is regenerated. Such behavior could reflect a combination of a need for more than one bound PIP_2 for activity, slow rebinding of PIP_2 to channels, or the involvement of other PIP_2-sensitive messenger signals. Working with $Ca_V2.1$ channels, Wu et al. (2002) considered a model with two PIP_2 binding sites, one with facilitatory and the other with inhibitory effects. Our experiments were done very differently from theirs, and our data are insufficient to discuss such details but we did not encounter any compelling evidence for inhibitory actions of PIP_2. The structure, number, and influences of PIP_2 binding sites on any ion channels are questions for future work, but as a working hypothesis we would consider a model with at least two facilitatory sites on the $Ca_V2.2$ channel complex both of which need to be occupied to see enhancement by PIP_2. That would make cooperative kinetics in which channel activity falls faster than PH domain FRET ratio during inhibition and rises more slowly than FRET ratio during recovery.

Conclusions

Slow modulation of Ca^{2+} channels by M_1 muscarinic receptors and more generally by any G_q-coupled receptor uses multiple signaling pathways. We employed a strategy that keeps the cell intact yet is able to vary membrane PIP_2 quickly with minimum production of other distracting messages, especially with a novel use of a voltage-dependent phosphatase. We compensated for effects of voltage-dependent inactivation of channels on the test current amplitudes. Depending on the channel subtype, such focused experiments demonstrate that 35-55% of the Ca^{2+} channel activity is supported by PIP_2 as a cofactor. The channels do not fail with acutely reduced PIP_2 but they definitely generate larger currents when PIP_2 is at its normal endogenous level. Activation of M_1Rs removes more current than just the PIP_2-dependent component, but the PIP_2-dependent component accounts for more than half of the muscarinic modulation. Our early proposal (Bernheim et al., 1991; Mathie et al., 1992; Hille, 1994) that slow modulation of KCNQ channels and L- and N-type channels in sympathetic ganglion cells share a common pathway is partly borne out. They do use a common pathway, but the Ca^{2+}-channel modulation also uses additional signals. In sum, the PIP_2 hypothesis has now been proven for four voltage-gated Ca^{2+} channel subtypes that are modulated by M_1 muscarinic receptors, and it has been shown not to apply to four other Ca_V subtypes that are not modulated by M_1 muscarinic receptors.

EXPERIMENTAL PROCEDURES

Cell Culture and Transfection

TsA201 cells (large-T-antigen transformed HEK 293 cells) were maintained in DMEM supplemented with 10% FBS and 0.2% penicillin/ streptomycin and transiently transfected using Lipofectamine 2000 (Invitrogen) with various cDNAs (See Supplementary Experimental procedures). For Ca^{2+} channel expression, cells were transfected with the α1 subunit of Ca_V, β3, and α2δ1 in a 1:1:1 molar ratio. When needed, 0.1 μg of cDNA encoding green fluorescent protein (GFP) or tetrameric red FP (DsRed) was co-transfected with the cDNA as a marker for successfully transfected cells. The next day, the cells were plated onto poly-L-lysine-coated coverslip chips, and fluorescent cells were studied within 1 - 2 days in FRET and electrophysiological experiments. Cultured SCG neurons were prepared as described (Mochida et al., 2003). Briefly, ganglia were dissected from 7-day

postnatal rats, desheathed, and incubated with collagenase (0.65 mg/ml; Worthington Biochemical) in L-15 medium (Gibco) at 37°C for 40min. Following enzyme treatment, ganglia were triturated gently through a small-pore glass pipette, washed twice by low speed centrifugation, and resuspended in DMEM supplemented with 10% fetal calf serum (Gibco), 5% horse serum (Gibco), 1% penicillin–streptomycin solution (Gibco), and 25 ng/ml nerve growth factor (2.5 S; Alomone Labs Ltd.). Cells were plated on glass coverslips coated with poly-D-lysine in 35mm dish incubated at 37°C (5% CO_2). cDNA encoding Dr-VSP was microinjected into the nuclei of SCG neurons through glass micropipettes one week after plating. Successful injection was monitored by 5% fast green dye in the nucleus. N-type currents were recorded two days after injection of cDNA.

Current Recording

The whole-cell configuration of the patch-clamp technique was used to voltage-clamp and dialyze cells at room temperature (22 - 25°C). Electrodes pulled from glass micropipette capillaries (Sutter Instrument, Novato, CA) had resistances of 1.3 - 2.5 MΩ. The whole-cell access resistance was 2 - 5 MΩ, and series-resistance errors were compensated > 60%. Fast and slow capacitance was compensated prior to the applied test-pulse sequences. Ba^{2+} currents were recorded by holding the cell at −70 mV or −80 mV and applying 10-ms (or 500-ms in Figure 9) test pulses to −10 mV or +10 mV to measure $Ca_V1.3$ and $Ca_V2.2$ or $Ca_V1.2$ currents, respectively. Note that tsA cells do not have endogenous voltage-gated Ca^{2+} channels and all the inward Ba^{2+} current was completely blocked by application of 30 μM Cd^{2+}. In the experiments with pipette solutions containing the ATP analogues AMP-PCP or AMP-PNP, we waited longer than 3 min before activating VSP proteins to allow time for the dialysis of the analogues into the cytoplasm.

Solutions and Materials

The external Ringer's solution used for Ba^{2+} current recording and photometry contained (in mM): 150 NaCl, 10 $BaCl_2$, 1 $MgCl_2$, 10 HEPES, and 8 glucose, adjusted to pH 7.4 with NaOH. The pipette solution contained (in mM): 175 CsCl, 5 $MgCl_2$, 5 HEPES, 0.1 1,2-bis(2-aminophenoxy)ethane *N*,*N*,*N'*,*N'*-tetraacetic acid (BAPTA), 3 Na_2ATP, and 0.1 Na_3GTP, titrated to pH 7.4 with CsOH. For current measurements through Ca^{2+} channels in SCG neurons, the bath solution contained (in mM) 162.5 tetraethylammonium (TEA) chloride, 5 $BaCl_2$, 10 HEPES, 8 glucose, 1 $MgCl_2$, 0.0001 TTX, and 0.005 nimodipine, pH adjusted to 7.4 with TEAOH. Variations on the solutions are noted in text. Reagents were obtained as follows: oxotremorine methiodide (Oxo-M) (Research Biochemicals, Natick, MA); BAPTA (Molecular Probes, Eugene, OR); DMEM, fetal bovine serum, lipofectamine 2000, and penicillin/streptomycin (Invitrogen, Carlsbad, CA); ATP, GTP, AMP-PCP, AMP-PNP, and other chemicals (Sigma, St. Louis, MO).

Epifluorescence Photometry

Fluorescence resonance energy transfer (FRET) between CFP and YFP was measured in single cells using an epifluorescence microscope equipped with two photomultipliers in photon-counting mode as described previously (Jensen et al., 2009). Cells were studied on the inverted microscope using a 40x, 1.3 numerical aperture oil-immersion objective. Excitation arc light passed through a 0.2 ND filter and a cube with a 440 ± 10 nm excitation filter and a 465 nm dichroic mirror. The total emitted light from the entire cell image was pooled and counted after deflection to the photomultiplier tubes by two cubes in series: a 505 nm dichroic mirror with a 480 ± 15 nm filter ("short-wavelength channel"), and a 570 nm dichroic mirror with a 535 ± 12.5 nm bandpass filter ("long-wavelength channel"). For sampling, the illumination shutter was opened for 24 ms every 500 ms. The fluorescence ratio was taken as the ratio of long-wavelength to short-wavelength emission (YFP_C/CFP_C) during 440 nm illumination after corrections for background fluorescence and bleedthrough

determined in separate experiments on cells transfected with single fluorophores. The subscript C is a reminder that the 440-nm excitation light is exciting CFP in both cases.

Data Analysis

Data acquisition and analysis used Pulse/Pulse Fit 8.11 software in combination with an EPC-9 patch clamp amplifier (HEKA, Lambrecht, Germany). Further data processing was performed with Excel (Microsoft, Bellevue, WA) and Igor Pro (WaveMetrics, Lake Oswego, OR). Time constants were measured by exponential fits. All quantitative data are expressed as the mean ± SEM. Comparison between two groups was analyzed using Student's t-test, and differences were considered significant at a level $P < 0.05$.

Supplementary Material

Refer to Web version on PubMed Central for supplementary material.

Acknowledgments

We are grateful to Drs. Sharona E Gordon, Todd Scheuer, Jill B Jensen, and Bjoern H Falkenburger for help with FRET approaches, valuable discussions, and comments on our manuscript, Lindsey A Burnett and Mark W Moody for plasmid amplification, and Lea M Miller for technical assistance. We thank many labs who supplied plasmids (see Supplementary procedures). This work was supported by National Institutes of Health Grant NS08174 (B.H.), NS0222625 (W.A. Catterall), and T32 GM07108 (K.L.).

REFERENCES

Agler HL, Evans J, Tay LH, Anderson MJ, Colecraft HM, Yue DT. G protein-gated inhibitory module of N-type ($Ca_V2.2$) Ca^{2+} channels. Neuron. 2005; 46:891–904. [PubMed: 15953418]

Bannister RA, Melliti K, Adams BA. Reconstituted slow muscarinic inhibition of neuronal (Ca_V 1.2c) L-type Ca^{2+} channels. Biophys. J. 2002; 83:3256–3267. [PubMed: 12496094]

Bean BP. Neurotransmitter inhibition of neuronal calcium currents by changes in channel voltage dependence. Nature. 1989; 340:153–156. [PubMed: 2567963]

Bell TJ, Thaler C, Castiglioni AJ, Helton TD, Lipscombe D. Cell-specific alternative splicing increases calcium channel current density in the pain pathway. Neuron. 2004; 41:127–138. [PubMed: 14715140]

Bernheim L, Beech DJ, Hille B. A diffusible second messenger mediates one of the pathways coupling receptors to calcium channels in rat sympathetic neurons. Neuron. 1991; 6:859–867. [PubMed: 1647174]

Brown DA, Hughes SA, Marsh SJ, Tinker A. Regulation of M (Kv7.2/7.3) channels in neurons by PIP_2 and products of PIP_2 hydrolysis: significance for receptor-mediated inhibition. J. Physiol. 2007; 582:917–925. [PubMed: 17395626]

Catterall WA. Structure and regulation of voltage-gated Ca^{2+} channels. Annu. Rev. Cell Dev. Biol. 2000; 16:521–555. [PubMed: 11031246]

Catterall WA, Perez-Reyes E, Snutch TP, Striessnig J. International Union of Pharmacology. XLVIII. Nomenclature and structure-function relationships of voltage-gated calcium channels. Pharmacol. Rev. 2005; 57:411–425. [PubMed: 16382099]

Delmas P, Coste B, Gamper N, Shapiro MS. Phosphoinositide lipid second messengers: new paradigms for calcium channel modulation. Neuron. 2005; 47:179–182. [PubMed: 16039560]

Dolphin AC. G protein modulation of voltage-gated calcium channels. Pharmacol. Rev. 2003; 55:607–627. [PubMed: 14657419]

Elmslie KS, Zhou W, Jones SW. LHRH and GTPγS modify calcium current activation in bullfrog sympathetic neurons. Neuron. 1990; 5:75–80. [PubMed: 2164405]

Gamper N, Reznikov V, Yamada Y, Yang J, Shapiro MS. Phosphatidylinositol 4,5-bisphosphate signals underlie receptor-specific $G_{q/11}$-mediated modulation of N-type Ca^{2+} channels. J. Neurosci. 2004; 24:10980–10992. [PubMed: 15574748]

Halaszovich CR, Schreiber DN, Oliver D. Ci-VSP is a depolarization-activated phosphatidylinositol-4,5-bisphosphate and phosphatidylinositol-3,4,5-trisphosphate 5′-phosphatase. J. Biol. Chem. 2009; 284:2106–2113. [PubMed: 19047057]

Herlitze S, Garcia DE, Mackie K, Hille B, Scheuer T, Catterall WA. Modulation of Ca^{2+} channels by G-protein βγ subunits. Nature. 1996; 380:258–262. [PubMed: 8637576]

Hille B. Modulation of ion-channel function by G-protein-coupled receptors. Trends Neurosci. 1994; 17:531–536. [PubMed: 7532338]

Horowitz LF, Hirdes W, Suh BC, Hilgemann DW, Mackie K, Hille B. Phospholipase C in living cells: activation, inhibition, Ca^{2+} requirement, and regulation of M current. J. Gen. Physiol. 2005; 126:243–262. [PubMed: 16129772]

Howe AR, Surmeier DJ. Muscarinic receptors modulate N-, P-, and L-type Ca^{2+} currents in rat striatal neurons through parallel pathways. J. Neurosci. 1995; 15:458–469. [PubMed: 7823150]

Ikeda SR. Voltage-dependent modulation of N-type calcium channels by G-protein βγ subunits. Nature. 1996; 380:255–258. [PubMed: 8637575]

Jensen JB, Lyssand JS, Hague C, Hille B. Fluorescence changes reveal kinetic steps of muscarinic receptor-mediated modulation of phosphoinositides and $K_V7.2/7.3$ K^+ channels. J. Gen. Physiol. 2009; 133:347–359. [PubMed: 19332618]

Lechner SG, Hussl S, Schicker KW, Drobny H, Boehm S. Presynaptic inhibition via a phospholipase C- and phosphatidylinositol bisphosphate-dependent regulation of neuronal Ca^{2+} channels. Mol. Pharmacol. 2005; 68:1387–1396. [PubMed: 16099842]

Lipscombe D, Kongsamut S, Tsien RW. Alpha-adrenergic inhibition of sympathetic neurotransmitter release mediated by modulation of N-type calcium-channel gating. Nature. 1989; 340:639–642. [PubMed: 2570354]

Lin Z, Harris C, Lipscombe D. The molecular identity of Ca channel α1-subunits expressed in rat sympathetic neurons. J. Mol. Neurosci. 1996; 7:257–267. [PubMed: 8968947]

Liu L, Rittenhouse AR. Arachidonic acid mediates muscarinic inhibition and enhancement of N-type Ca^{2+} current in sympathetic neurons. Proc. Natl. Acad. Sci. USA. 2003; 100:295–300. [PubMed: 12496347]

Liu L, Zhao R, Bai Y, Stanish LF, Evans JE, Sanderson MJ, Bonventre JV, Rittenhouse AR. M_1 muscarinic receptors inhibit L-type Ca^{2+} current and M-current by divergent signal transduction cascades. J. Neurosci. 2006; 26:11588–11598. [PubMed: 17093080]

Mathie A, Bernheim L, Hille B. Inhibition of N- and L-type calcium channels by muscarinic receptor activation in rat sympathetic neurons. Neuron. 1992; 8:907–914. [PubMed: 1316767]

Melliti K, Meza U, Adams BA. RGS2 blocks slow muscarinic inhibition of N-type Ca^{2+} channels reconstituted in a human cell line. J. Physiol. 2001; 532:337–347. [PubMed: 11306654]

Michailidis IE, Zhang Y, Yang J. The lipid connection-regulation of voltage-gated Ca^{2+} channels by phosphoinositides. Pflugers Arch. 2007; 455:147–155. [PubMed: 17541627]

Mochida S, Westenbroek RE, Yokoyama CT, Itoh K, Catterall WA. Subtype-selective reconstitution of synaptic transmission in sympathetic ganglion neurons by expression of exogenous Ca^{2+} channels. Proc. Natl. Acad. Sci. USA. 2003; 100:2813–2818. [PubMed: 12601155]

Murata Y, Iwasaki H, Sasaki M, Inaba K, Okamura Y. Phosphoinositide phosphatase activity coupled to an intrinsic voltage sensor. Nature. 2005; 435:1239–1243. [PubMed: 15902207]

Okamura Y, Murata Y, Iwasaki H. Voltage-sensing phosphatase: actions and potentials. J. Physiol. 2009; 587:513–520. [PubMed: 19074969]

Raingo J, Castiglioni AJ, Lipscombe D. Alternative splicing controls G protein-dependent inhibition of N-type calcium channels in nociceptors. Nat. Neurosci. 2007; 10:285–292. [PubMed: 17293861]

Roberts-Crowley ML, Mitra-Ganguli T, Liu L, Rittenhouse AR. Regulation of voltage-gated Ca^{2+} channels by lipids. Cell Calcium. 2009; 45:589–601. [PubMed: 19419761]

Shapiro MS, Roche JP, Kaftan EJ, Cruzblanca H, Mackie K, Hille B. Reconstitution of muscarinic modulation of the KCNQ2/KCNQ3 K^+ channels that underlie the neuronal M current. J. Neurosci. 2000; 20:1710–1721. [PubMed: 10684873]

Suh BC, Hille B. Recovery from muscarinic modulation of M current channels requires phosphatidylinositol 4,5-bisphosphate synthesis. Neuron. 2002; 35:507–520. [PubMed: 12165472]

Suh BC, Hille B. Electrostatic interaction of internal Mg^{2+} with membrane PIP_2 seen with KCNQ K^+ channels. J. Gen. Physiol. 2007; 130:241–256. [PubMed: 17724161]

Suh BC, Hille B. PIP_2 is a necessary cofactor for ion channel function: how and why? Annu. Rev. Biophys. 2008; 37:175–195. [PubMed: 18573078]

Suh BC, Inoue T, Meyer T, Hille B. Rapid chemically induced changes of PtdIns(4,5)P_2 gate KCNQ ion channels. Science. 2006; 314:1454–1457. [PubMed: 16990515]

van der Wal J, Habets R, Várnai P, Balla T, Jalink K. Monitoring agonist-induced phospholipase C activation in live cells by fluorescence resonance energy transfer. J. Biol. Chem. 2001; 276:15337–15344. [PubMed: 11152673]

Willars GB, Nahorski SR, Challiss RA. Differential regulation of muscarinic acetylcholine receptor-sensitive polyphosphoinositide pools and consequences for signaling in human neuroblastoma cells. J. Biol. Chem. 1998; 273:5037–5046. [PubMed: 9478953]

Winks JS, Hughes S, Filippov AK, Tatulian L, Abogadie FC, Brown DA, Marsh SJ. Relationship between membrane phosphatidylinositol-4,5-bisphosphate and receptor-mediated inhibition of native neuronal M channels. J. Neurosci. 2005; 25:3400–3413. [PubMed: 15800195]

Varnai P, Thyagarajan B, Rohacs T, Balla T. Rapidly inducible changes in phosphatidylinositol 4,5-bisphosphate levels influence multiple regulatory functions of the lipid in intact living cells. J. Cell Biol. 2006; 175:377–382. [PubMed: 17088424]

Wenk MR, Pellegrini L, Klenchin VA, Di Paolo G, Chang S, Daniell L, Arioka M, Martin TF, De Camilli P. PIP kinase Iγ is the major PI(4,5)P_2 synthesizing enzyme at the synapse. Neuron. 2001; 32:79–88. [PubMed: 11604140]

Wu L, Bauer CS, Zhen XG, Xie C, Yang J. Dual regulation of voltage-gated calcium channels by PtdIns(4,5)P_2. Nature. 2002; 419:947–952. [PubMed: 12410316]

Zamponi GW, Snutch TP. Decay of prepulse facilitation of N type calcium channels during G protein inhibition is consistent with binding of a single Gβ subunit. Proc. Natl. Acad. Sci. USA. 1998; 95:4035–4039. [PubMed: 9520488]

Zhang H, Craciun LC, Mirshahi T, Rohács T, Lopes CM, Jin T, Logothetis DE. PIP_2 activates KCNQ channels, and its hydrolysis underlies receptor-mediated inhibition of M currents. Neuron. 2003; 37:963–975. [PubMed: 12670425]

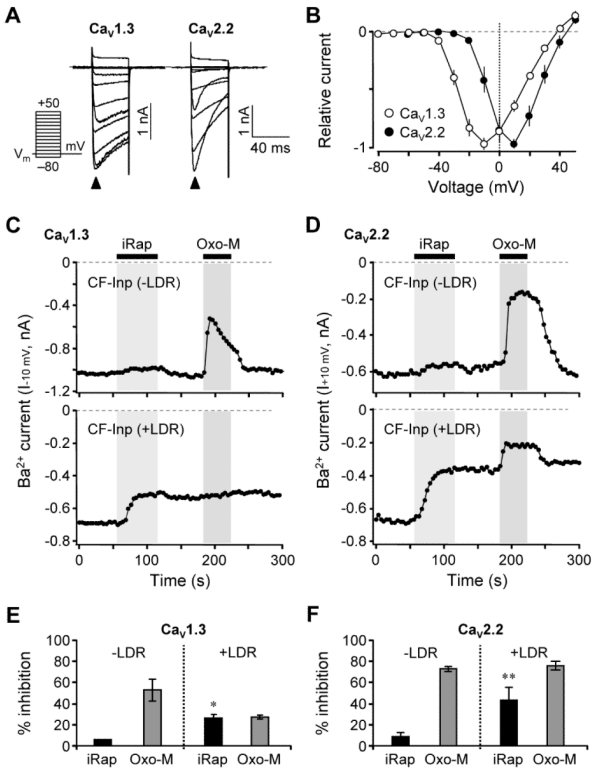

Figure 1. PIP$_2$ Depletion Depresses Ca$_V$1.3 and Ca$_V$2.2 Voltage-Gated Ba^{2+} Currents

(A) Families of whole-cell Ba^{2+} currents elicited by voltage steps from −80 to +50 mV in 10-mV intervals (see pulse protocol), in cells expressing Ca$_V$1.3 (left) and Ca$_V$2.2 (right) channels. Holding potential is −70 mV and dashed line is zero current. Closed arrowheads indicate peak inward Ba^{2+} currents triggered by the depolarizing test pulses. Tail currents are clipped.

(B) Peak current-voltage (I-V) relations for Ca$_V$1.3 and Ca$_V$2.2 currents in whole-cell recording normalized to the maximum current. Points are mean ± SEM (Ca$_V$1.3, n = 6; Ca$_V$2.2, n = 8).

(C and D) Current modulation by iRap (5 μM) and Oxo-M (10 μM) in cells co-expressing M$_1$ muscarinic receptors and CF-Inp alone (top, −LDR) or with LDR (bottom, +LDR). Currents were recorded in response to test pulses to −10 mV (Ca$_V$1.3) or +10 mV (Ca$_V$2.2) every 4 s. Dashed line is zero current. LDR, membrane anchor protein. CF-Inp, PI 5-phosphatase.

(E and F) Percent inhibition of Ca$_V$1.3 (E) and Ca$_V$2.2 (F) currents by iRap and Oxo-M compared to initial currents in cells expressing CF-Inp alone (−LDR) or with LDR (+LDR). The application of iRap significantly inhibited Ca$_V$1.3 currents (*P < 0.05 compared to iRap effect without LDR, n = 3 for −LDR; n = 4 for +LDR) and Ca$_V$2.2 currents (**P < 0.01 compared to iRap effect without LDR, n = 3 for both −LDR and +LDR). Data are mean ± SEM. See also Figure S1.

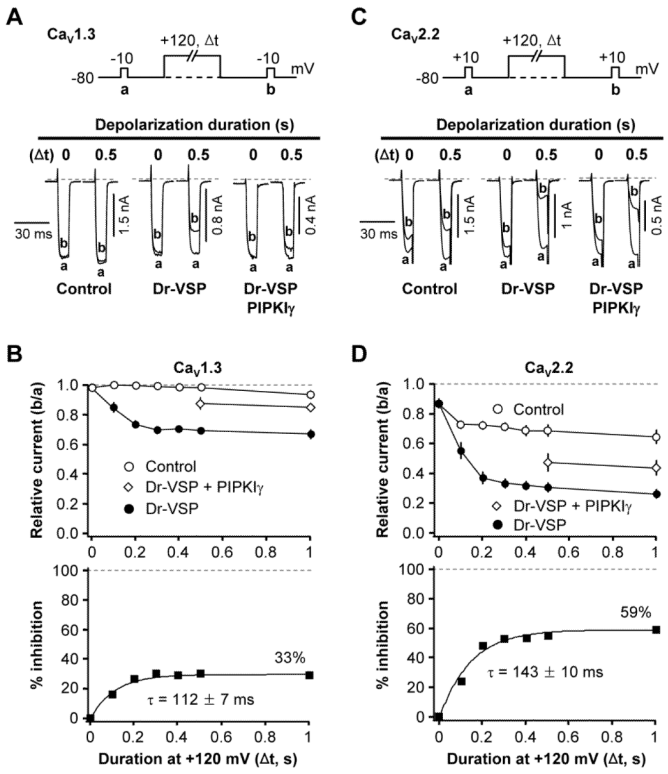

Figure 2. Inhibition of Ca_V Currents by Dr-VSP-Mediated PIP_2 Depletion

(A and C) Typical traces of $Ca_V1.3$ (A) and $Ca_V2.2$ (C) currents before and after activation of Dr-VSP by depolarizations to +120 mV. Cells without Dr-VSP (Control), cells transfected with Dr-VSP, or cells transfected with Dr-VSP plus PIPKIγ received a test pulse to −10 (A) or +10 mV (C) for 10 ms and then were depolarized to +120 mV for zero or 0.5 s (as marked), followed by a second test-pulse. The currents before (a) and after (b) the +120 mV-depolarizing pulse are superimposed. Dashed line is zero current.

(B and D) Time-dependent inhibition of L-type ($Ca_V1.3$, B) and N-type ($Ca_V2.2$, D) currents by Dr-VSP activation. Top, cells were depolarized to +120 mV for various times and the relative current ratio (b/a) was measured in control (open circle, n = 6-14 for $Ca_V1.3$ and n = 6 for $Ca_V2.2$), Dr-VSP-expressing (closed circle, n = 6-11 for $Ca_V1.3$ and n = 6 for $Ca_V2.2$) cells, and Dr-VSP plus PIPKIγ expressing cells (n = 5-8). The delay between subsequent test pulses was 1 min. Bottom, percent inhibition of currents by time-graded activation of Dr-VSP at +120 mV. See formula in text. The current inhibition by 1-s depolarizing pulse is labeled in each figure. See also Figure S2.

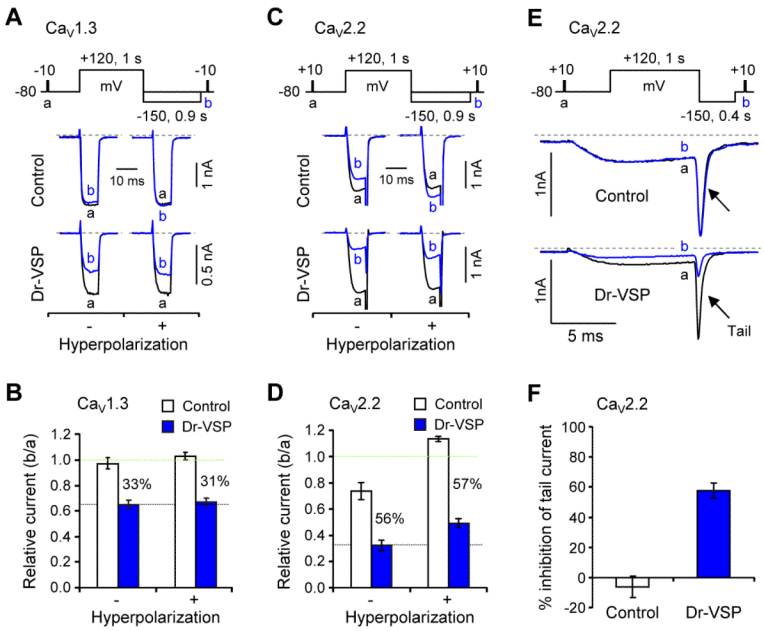

Figure 3. Channel Inhibition by Dr-VSP Corrected for VDI

(A and C) Effect of membrane hyperpolarization on Dr-VSP-induced inhibition of $Ca_V1.3$ (A) and $Ca_V2.2$ (C) currents. The changes of $Ca_V1.3$ and $Ca_V2.2$ currents by a +120-mV depolarizing pulse were measured without (−) and with (+) a hyperpolarizing step (−150 mV, 0.9 s) in control and Dr-VSP-expressing cells. Pairs of current traces were recorded from the same cell with a 1-min interval.

(B and D) Summary of the relative peak current (b/a) of $Ca_V1.3$ (B) and $Ca_V2.2$ (D) in control and Dr-VSP-expressing cells with and without the hyperpolarizing step. Data are mean ± SEM ($Ca_V1.3$, n = 5 - 6; $Ca_V2.2$, n = 4). The percent difference between control and Dr-VSP is labeled in each condition.

(E) Effect of Dr-VSP on $Ca_V2.2$ tail currents. Tail currents were measured with a hyperpolarizing step (−150 mV, 0.4 s) in control and Dr-VSP-expressing cells. Pairs of current traces were recorded from the same cell 1 min apart. Capacitive and leak currents were subtracted by a P/5 procedure.

(F) Summary of the tail-current inhibition (%) of $Ca_V2.2$ in control and Dr-VSP-expressing cells. Data are mean ± SEM (control, −6.1 ± 7.2, n = 5; Dr-VSP, 57.6 ± 5.2, n = 8).

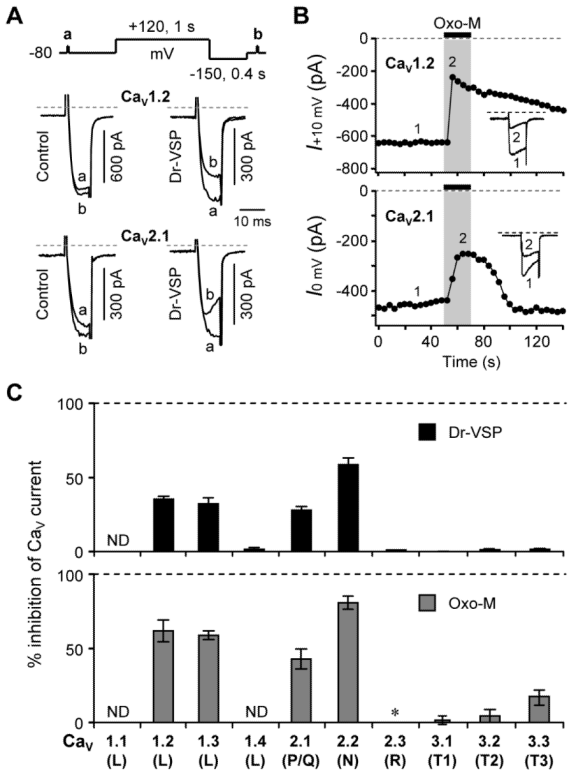

Figure 4. Screening Ca$_V$ Subtypes for Modulation by Dr-VSP and M$_1$ Muscarinic Receptors

(A) Inhibition of Ca$_V$1.2 and 2.1 currents by Dr-VSP-induced PIP$_2$ depletion. Ca$_V$ currents were measured during test pulses before and after a +120-mV/1-s depolarizing pulse in control and Dr-VSP-expressing cells. Typical current traces for each channel type are superimposed.

(B) Inhibition of Ca$_V$1.2 and 2.1 currents by M$_1$ muscarinic receptor stimulation with Oxo-M (10 μM). Insets, Typical traces before and after Oxo-M application were superimposed.

(C) Inhibition of Ca$_V$ currents by Dr-VSP-induced PIP$_2$ depletion (top) and M$_1$ muscarinic receptor stimulation with Oxo-M (B). ND, not determined. *The Ca$_V$2.3 current was enhanced 2.7 ± 0.5-fold (n = 4) by the activation of M$_1$ receptors. See also Figure S4.

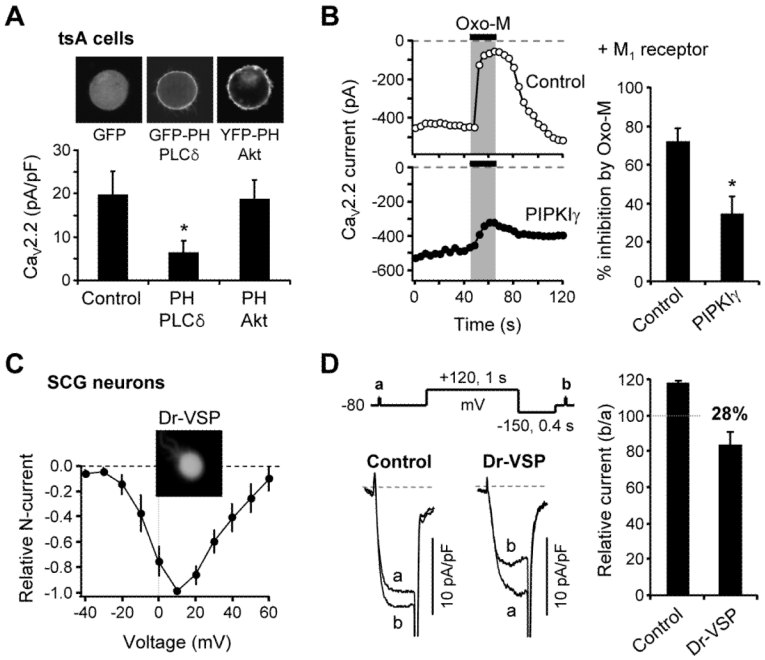

Figure 5. PIP_2-Dependent Modulation of $Ca_V2.2$ N-type channels

(A) $Ca_V2.2$ current density (pA/pF) was measured in cells expressing the $Ca_V2.2$ channels plus GFP, GFP-PH-PLCδ1, or YFP-PH-Akt. The cells were transfected with the same amounts of cDNA. Average membrane capacitances for cells are 22 ± 2 pF for GFP (n = 11), 25 ± 4 for PH-PLC (n = 11), and 24 ± 4 for PH-Akt (n = 12). Top, Confocal images of tsA cells expressing each fluorescent protein. Cell diameters were 20 - 30 μm.

(B) Elevated PIP_2 levels attenuate $Ca_V2.2$ channel inhibition by M_1 receptor stimulation. $Ca_V2.2$ currents were measured in control cells and in cells transfected with PIPKIγ. Right, Summary of current inhibition by Oxo-M. Data are mean ± SEM. *P < 0.05, compared to control.

(C) Current-voltage (I-V) relations of N-type Ca_V current in isolated rat SCG neurons expressing Dr-VSP (n = 3) with a widefield image of one neuron.

(D) Inhibition of N-type Ca_V currents by Dr-VSP activation in SCG neurons. N-type Ca_V currents were measured during test pulses before and after a +120-mV/1-s depolarizing pulse in control and cells expressing Dr-VSP. Capacitive and leak currents were subtracted by a P/5 procedure. Right, Summary of N-type current inhibition by Dr-VSP activation in SCG neurons. Data are mean ± SEM (n = 3 for control, n = 3 for Dr-VSP).

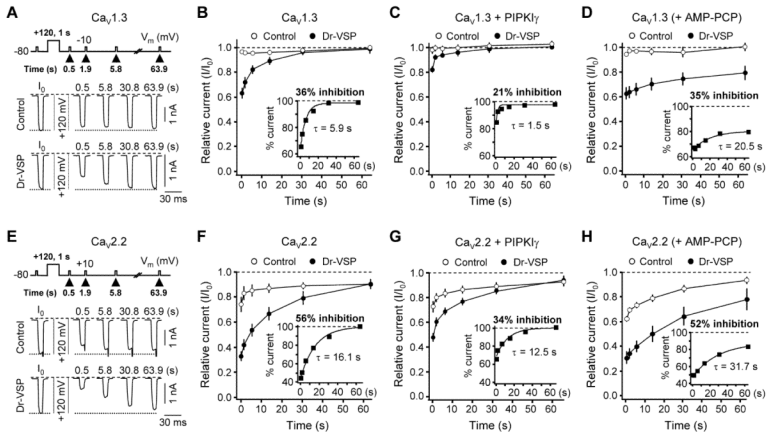

Figure 6. Recovery of Ca_V Currents after Dr-VSP-Induced Inhibition

(A and E) Current traces for $Ca_V1.3$ (A) and $Ca_V2.2$ (E) channels in control (top) and Dr-VSP-expressing (bottom) cells before and after a +120-mV/1-s depolarizing pulse. $Ca_V1.3$ and $Ca_V2.2$ currents were measured at −10 mV and +10 mV, respectively, at the indicated times after the +120-mV pulse. Dashed lines indicate zero current, and dotted lines, the initial Ca_V current before the depolarization step.

(B and F) Time course of recovery of $Ca_V1.3$ and $Ca_V2.2$ currents after the Dr-VSP-induced inhibition in control (open circles) and Dr-VSP-expressing (closed circles) cells. Data are mean ± SEM ($Ca_V1.3$, n = 6 for both control and Dr-VSP; $Ca_V2.2$, n = 5 for both). Inset shows % current relative to control cells.

(C and G) Time course of $Ca_V1.3$ and $Ca_V2.2$ current recovery in cells transfected with PIPKIγ ($Ca_V1.3$, n = 5 for control and n = 8 for Dr-VSP; $Ca_V2.2$, n = 4 for control and n = 5 for Dr-VSP). Inset shows % current, comparing Dr-VSP to control cells.

(D and H) Time course of $Ca_V1.3$ and $Ca_V2.2$ current recovery with 3 mM AMP-PCP instead of ATP in the pipette solution. Data are mean ± SEM ($Ca_V1.3$, n = 7 for control and n = 10 for Dr-VSP; $Ca_V2.2$, n = 6 for control and n = 5 for Dr-VSP). Insets show the % current recovery in the presence of AMP-PCP. See also Figure S4.

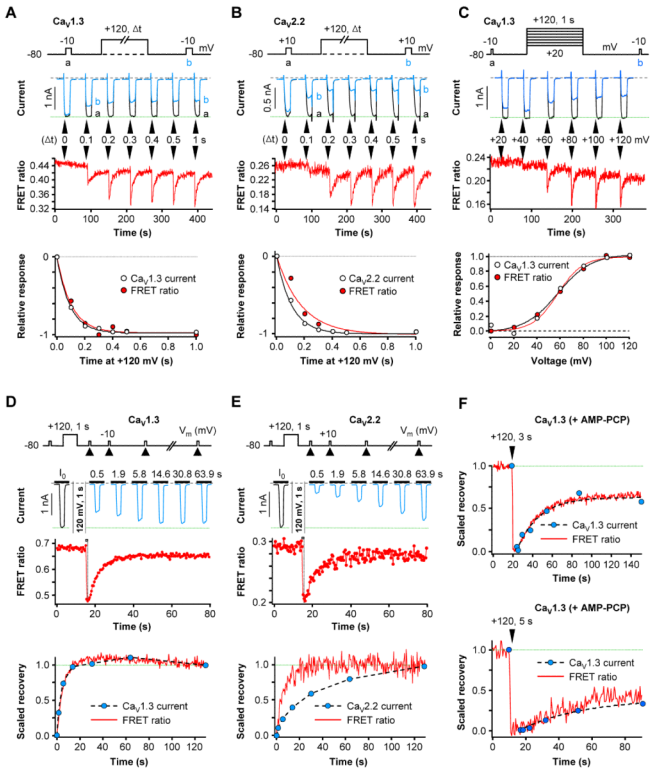

Figure 7. Simultaneous Measurement of Ca_V Current Modulation and PIP_2 Depletion in Single Cells

All cells co-express channel subunits, PH-domain probes, and Dr-VSP. (A and B) Single-cell measurements of FRET ratio signals and whole-cell current from $Ca_V1.3$ (A) or $Ca_V2.2$ (B) channels. Top, Time-dependent induction of Dr-VSP effect on current and FRET ratio measured simultaneously in single cells. Bottom, superimposed time courses of current inhibition and FRET ratio decrease, normalized.

(C) Voltage dependence of Dr-VSP action on $Ca_V1.3$ current and FRET ratio change in a single cell.

(D and E). Time course of recovery of FRET ratio signals and whole-cell current of $Ca_V1.3$ (E) or $Ca_V2.2$ (F) channels in single-cell experiments. Top, recovery of currents and FRET ratio from the Dr-VSP-induced changes was measured simultaneously in single cells. Bottom, superimposed recoveries of current and FRET ratio in a single cell.

(F) AMP-PCP in the pipette solution attenuates the recovery of $Ca_V1.3$ current and FRET ratio. A single cell dialyzed with 3 mM AMP-PCP was given a 3-s or 5-s depolarizing pulse and current and FRET ratio were measured simultaneously.

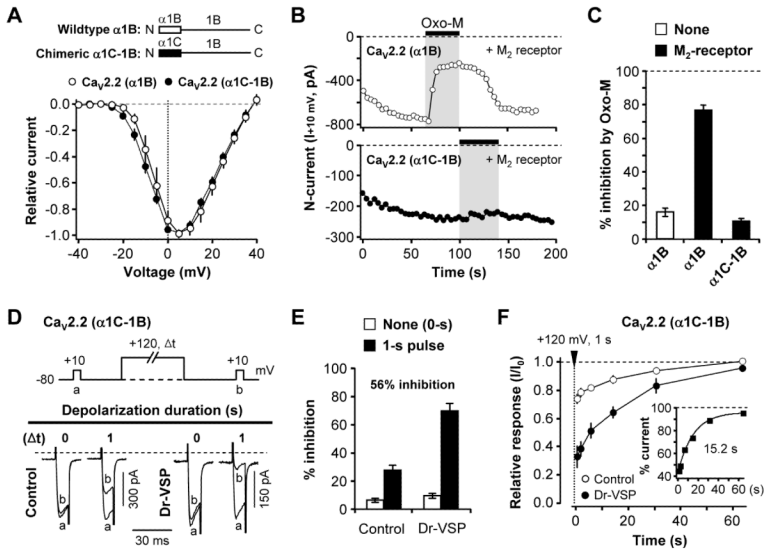

Figure 8. Modulation by Dr-VSP in a Gβγ-Insensitive Chimeric Ca$_V$2.2 Channel

(A) Normalized peak current-voltage (I-V) relations of wildtype Ca$_V$2.2 (α1B) and chimeric Ca$_V$2.2 (α1C-1B) channels in the whole-cell configuration. Currents were elicited by voltage-steps from −40 to +40 mV, in 5 mV intervals, from a holding potential of −80 mV. Points are mean ± SEM (n = 5 for both channels).

(B) Time course of M_2 muscarinic receptor action (Oxo-M, 10 μM) on wild type Ca$_V$2.2 (α1B) (top) or Ca$_V$2.2 (α1C-1B) (bottom) channels. The current amplitude was measured at +10 mV every 4 s.

(C) Summary of the muscarinic inhibition of Ca$_V$2.2 (α1B) and Ca$_V$2.2 (α1C-1B) currents by M_2Rs. Data are mean ± SEM (Ca$_V$2.2 (α1B) alone, n = 5; Ca$_V$2.2 (α1B) with M_2 receptors, n = 4; Ca$_V$2.2 (α1C-1B) with M_2 receptor, n = 5).

(D) Inhibition of chimeric Ca$_V$2.2 (α1C-1B) currents by Dr-VSP. Typical traces of Ca$_V$2.2 (α1C-1B) currents before and after Dr-VSP activation by depolarization to +120 mV. Control (left) and Dr-VSP-expressing (right) cells received a test pulse and then were depolarized to +120 mV for zero or 1 s (Δt), followed by the second test pulse (b). The currents before (a) and after (b) the depolarizing pulse superimposed.

(E) Summary of the current inhibition (%) by the +120-mV depolarizing pulse in control (n = 8) and Dr-VSP-expressing (n = 5) cells.

(F) Time course of current recovery from Dr-VSP-induced inhibition. Cells were depolarized to +120 mV for 1 s, and the recovery of currents was measured. Inset shows the percent current from comparing control and Dr-VSP-expressing cells. Data are mean ± SEM (n = 6).

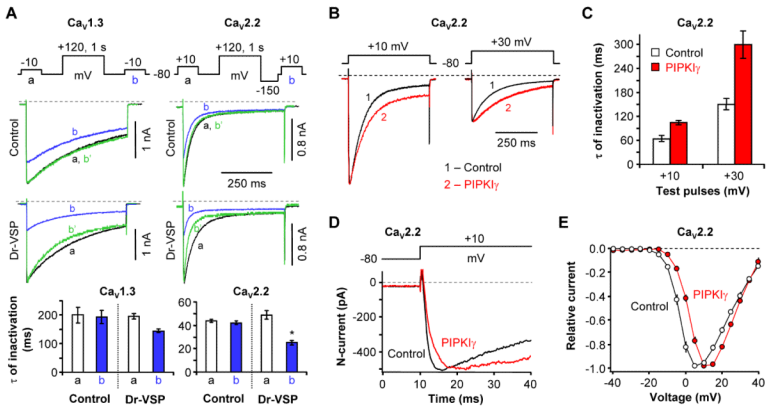

Figure 9. PIP$_2$ Depletion Affects Channel Inactivation and Activation

(A) Effect of Dr-VSP-induced PIP$_2$ depletion on the rate of inactivation of Ca$_V$1.3 (left) and Ca$_V$2.2 (right) currents. Ca$_V$ currents were measured during 500-ms test pulses to −10 (Ca$_V$1.3) or +10 mV (Ca$_V$2.2) before (a) and after (b) a +120-mV/1-s depolarizing pulse in control cells (top) and in cells expressing Dr-VSP (bottom). Green lines (b') are b current traces scaled to the peak amplitude of a current. Bottom, summary of the time constants for current inactivation (n = 5, *P < 0.01, compared to current a).

(B) Elevated PIP$_2$ levels slow Ca$_V$2.2 channel inactivation. Ca$_V$2.2 currents during 500-ms test pulses to +10 mV or +30 mV were measured in control cells with no Dr-VSP and in cells transfected with PIPKIγ. Typical current traces for each test voltage are overlaid.

(C) Summary of inactivation time constants (τ) for Ca$_V$2.2 current during the +10-mV and +30-mV test pulses with different PIP$_2$ levels in the plasma membrane. Data are mean ± SEM (n = 5 for control, n = 7 for PIPKIγ at both test pulses).

(D) Elevated PIP$_2$ levels slow Ca$_V$2.2 channel activation. Activation of Ca$_V$2.2 channels during the depolarization to +10 mV was measured in control cells with no Dr-VSP and in cells co-transfected with PIPKIγ. Currents showing similar amplitude are superimposed.

(E) Current–voltage (I-V) relations of Ca$_V$2.2 channels in control (open circle) and PIPKIγ-transfected (closed circle) cells. Relative currents are plotted against test potential. Points are mean ± SEM (n = 8 for control; n = 9 for PIPKIγ). See also Figure S5.